Journal of
Ceramic Science
and Technology

J. Ceram. Sci. Technol., 09 [4] 371-380 (2018)
DOI: 10.4416/JCST2018-00015
available online at: http://www.ceramic-science.com

Estimation of fiber/matrix interfacial friction coefficient in continuous fiber-reinforced ceramic-matrix composites at room and elevated temperatures under cyclic loading

L. Li*

College of Civil Aviation, Nanjing University of Aeronautics and Astronautics No.29 Yudao St., Nanjing 210016, PR China

received Febuary 23, 2018; received in revised form April 4, 2018; accepted April 27, 2018

Abstract

In this paper, the fiber/matrix interfacial frictional coefficient of continuous fiber-reinforced ceramic-matrix composites (CMCs) at room and elevated temperatures have been investigated. The fatigue hysteresis loops models considering the fiber/matrix interface friction between fibers and the matrix have been developed to establish the relationships between the fatigue hysteresis loops, fatigue hysteresis dissipated energy and fiber/matrix interface frictional coefficient. Using the experimental fatigue hysteresis dissipated energy, the fiber/matrix interface frictional coefficient of SiC/Si_3N_4 and SiC/SiC composites at room and elevated temperatures were obtained for different cycle numbers, interface properties and fatigue peak stresses. The effects of fiber/matrix interface bonding, fatigue peak stress, test temperature and cycle number on the evolution of fatigue hysteresis dissipated energy and fiber/matrix interface frictional coefficient have been analyzed.

Keywords: *Ceramic-matrix composites (CMCs); fatigue; interface debonding; interface frictional coefficient.*

I. Introduction

Ceramic-matrix composites (CMCs) possess a high specific modulus and specific strength at elevated temperatures, and have already been applied in hot-section components in military and commercial aero engines [1]. In order to meet the airworthiness certification requirements, it is necessary to analyze the damage mechanisms when the CMCs are subjected to cyclic loading and to develop the models, methods and tools to predict the damage development and fatigue life of CMCs [2].

When matrix cracking and fiber/matrix interface debonding occur, the fiber/matrix interface shear stress transfers load, which is critical for the non-linear behavior of CMCs. Upon unloading and subsequent reloading, the fiber/matrix interface shear stress degrades with applied cycles, which affects inelastic strain and the ultimate tensile strength [3, 4, 5]. Several approaches are currently used to determine the interface shear stress along the fiber/matrix interface, i.e. fiber pullout [6], fiber push-in [7] and push-out [8], and so on. However, there are some disadvantages in these approaches. Firstly, they can only obtain the individual fiber's interface properties; secondly, it is difficult to measure the interface properties at elevated temperature; thirdly, these approaches can only provide information regarding the interface shear stress that would exist under monotonic loading conditions. By assuming the constant fiber/matrix interface shear stress along the loading direction between the fiber and the matrix, Li et al. [9] developed an approach to estimate the fiber/matrix interface shear stress of CMCs from hysteresis loops. It was found that the interface shear stress degradation rate increases with fatigue peak stress, and is much higher at low loading frequency and elevated temperature in oxidative environment. Solti et al. [10] proposed a means of inferring the state of the interface based on comparison of experimental and theoretical hysteresis loss energy on a cycle-by-cycle basis. Li et al. [11] investigated the fatigue hysteresis behavior of unidirectional SiC/Si_3N_4 composite at room temperature. Owing to the Poisson effect in fibers upon unloading and reloading, the fiber/matrix interface shear stress changes along the loading direction [12]. Li et al. [13] developed an approach to estimate the fiber/matrix interface frictional coefficient of CMCs from hysteresis loops. However, the evolution of the fiber/matrix interface frictional coefficient with increasing applied cycles at elevated temperatures has not been investigated.

In this paper, the estimation of the fiber/matrix interface frictional coefficient of unidirectional and 2D CMCs at room and elevated temperatures is investigated. Fatigue hysteresis loops models considering the fiber/matrix interface friction between fibers and the matrix are developed to establish the relationship between the fatigue hysteresis loops, fatigue hysteresis energy dissipation and the fiber/matrix interface frictional coefficient. The damage evolution process under cyclic fatigue loading is analyzed based on the fatigue hysteresis loops. The effects of fiber/matrix interface bonding, fatigue peak stress, test temperature and applied cycle number on the evolution of fatigue hysteresis dissipated energy and fiber/matrix interface frictional coefficient are analyzed.

* Corresponding author: llb451@nuaa.edu.cn

II. Hysteresis Theories

If matrix multicracking and fiber/matrix interface debonding occur, the fatigue stress/strain hysteresis loops develop as a result of fiber/matrix interface frictional sliding [14–17]. The shape, location and area of fatigue stress/strain hysteresis loops depend on the matrix multicracking, fiber/matrix interface debonding, interface wear at room temperature or interface oxidation at elevated temperature.

When the fiber/matrix interface partially debonds, the interface debonded region can be divided into the interface counter-slip region and the interface slip region upon unloading; and upon reloading, the interface debonded region can be divided into three regions, i.e. interface new-slip region, interface counter-slip region and interface slip region, as shown in Fig. 1. The unloading and reloading stress-strain relationships can be determined using the following equations.

$$\varepsilon_{c\_pu} = \frac{\sigma}{V_f E_f} - \frac{2\alpha v_f(\overline{\sigma} - \sigma)}{\lambda V_f E_f l_c(\alpha v_f + \gamma v_m)}(1 - 2e^{-\lambda y} + e^{\lambda(l_d - 2y)}) + \frac{\alpha v_f(\overline{\sigma} - \sigma)}{V_f E_f(\alpha v_f + \gamma v_m)}[1 - e]^{\lambda(l_d - 2y)}(1 - 2l_d/l_c) \quad (1)$$

$$\varepsilon_{c\_pr} = \frac{\sigma}{V_f E_f} - \frac{4\alpha v_f(\overline{\sigma} - \sigma)}{\lambda V_f E_f l_c(\alpha v_f + \gamma v_m)}(e^{\lambda z} - e^{-\lambda(y-2z)} + e^{\lambda(l_d - 2y + 2z)} - 1) + \frac{\alpha v_f(\overline{\sigma} - \sigma)}{V_f E_f(\alpha v_f + \gamma v_m)}[1 - e^{\lambda(L_d - 2y + 2z)}(1 - 2l_d/l_c)] \quad (2)$$

where v_f and v_m denote the fiber and matrix Poisson ratio, respectively; $\alpha = E_m/E_f$, E_m and E_f denote the matrix and fiber elastic modulus, respectively; $\gamma = V_f/V_m$, V_m and V_f denote the matrix and fiber volume fraction, respectively; l_d denotes the fiber/matrix interface debonded length; y and z denote the fiber/matrix interface counter-slip and new-slip length; λ and β denote the fiber/matrix interface slip length parameters; and $\overline{\sigma}$ denotes the fiber/matrix interface slip stress parameter.

When the fiber/matrix interface completely debonds, the interface debonded region of l_d occupies the entire matrix crack spacing of $l_c/2$, i.e. $l_d = l_c/2$. The unloading and reloading stress-strain relationships can be determined using the following equations.

$$\varepsilon_{c\_fu} = \frac{\sigma}{V_f E_f} + \frac{\alpha v_f(\overline{\sigma} - \sigma)}{V_f E_f(\alpha v_f + \gamma v_m)} - \frac{2\alpha v_f(\overline{\sigma} - \sigma)}{\lambda V_f E_f l_c(\alpha v_f + \gamma v_m)}(1 - 2e^{-\lambda y} + e^{\lambda(l_c/2 - 2y)}) \quad (3)$$

$$\varepsilon_{c\_fr} = \frac{\sigma}{V_f E_f} + \frac{\alpha v_f(\overline{\sigma} - \sigma)}{V_f E_f(\alpha v_f + \gamma v_m)} - \frac{2\alpha v_f(\overline{\sigma} - \sigma)}{\lambda V_f E_f l_c(\alpha v_f + \gamma v_m)}(2e^{\lambda z} - 2e^{-\lambda(y - 2z)} + e^{\lambda(l_c/2 - 2y + 2z)} - 1) \quad (4)$$

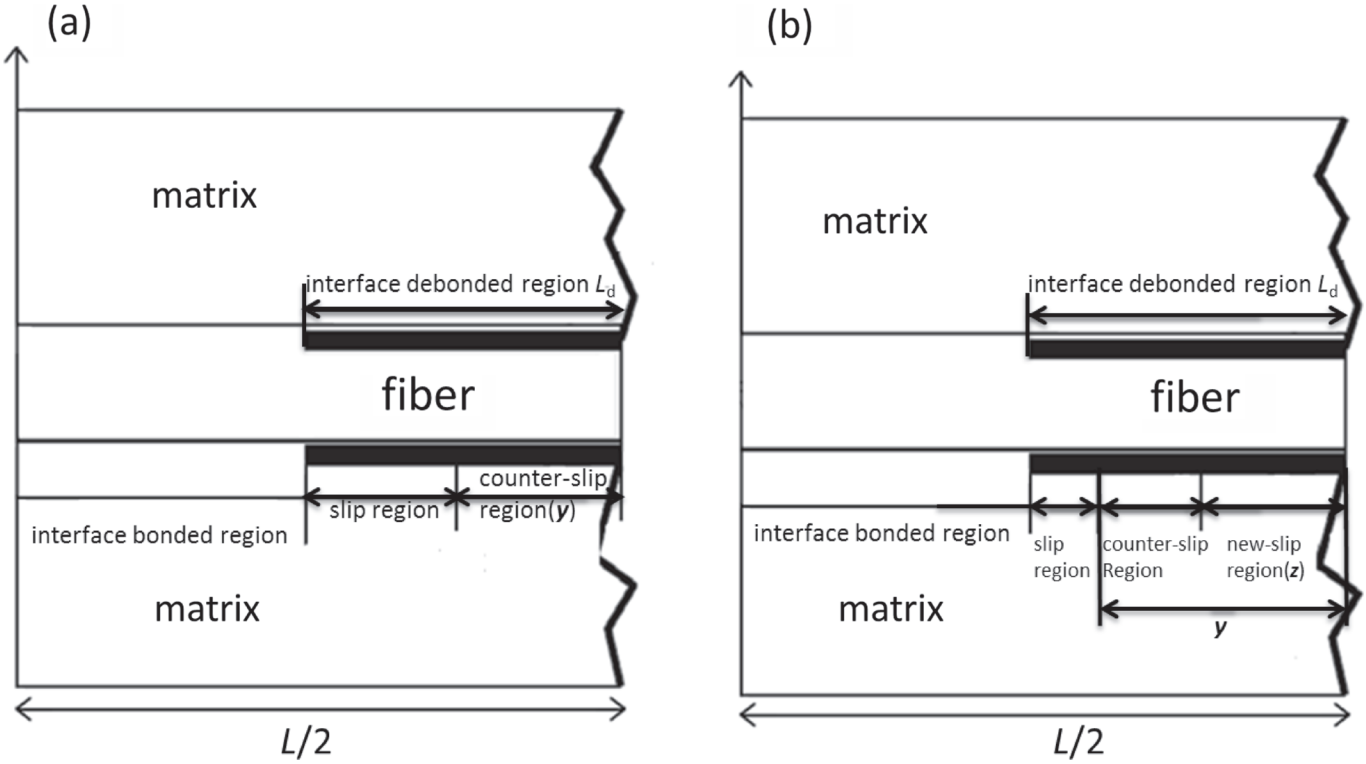

Fig. 1: The schematic figure showing fiber slipping relative to matrix upon (a) unloading; and (b) reloading.

Under cyclic fatigue loading, the area associated with the stress/strain hysteresis loops is the energy lost during the corresponding cycle, which is defined using the following equation.

$$U = \int_{\sigma_{min}}^{\sigma_{max}} [\varepsilon_c^{unload}(\sigma) - \varepsilon_c^{reload}(\sigma)]d\sigma \quad (5)$$

The fatigue hysteresis dissipated energy can be derived by inserting corresponding unloading and reloading strains into Eq. (5).

III. Experimental Comparisons

The evolution of experimental fatigue hysteresis loops, fatigue hysteresis dissipated energy and fiber/matrix interface frictional coefficient of SiC/Si_3N_4 and SiC/SiC composites at room and elevated temperatures are analyzed using the present analysis.

(1) Unidirectional SiC/Si_3N_4 composite

(a) *Room temperature*

Olivier [18] investigated the cyclic tension-tension fatigue behavior of unidirectional SiC/Si_3N_4 composite at room temperature. The fatigue tests were performed under load control at a triangular waveform with the loading frequency of 1.0 Hz and the fatigue load ratio (i.e. minimum to maximum stress) of zero, and the maximum number of applied cycles was defined to be 1000000 applied cycles.

For type A SiC/Si_3N_4 with strong fiber/matrix interface bonding at the fatigue peak stress of $\sigma_{max} = 460$ MPa, the experimental and predicted fatigue hysteresis loops at the cycle number of N = 1, 600, 10000 and 1000000 are shown in Fig. 2(a), with the corresponding fiber/matrix interface frictional coefficient of $\mu = 0.28$, 0.18, 0.14 and 0.08. The fatigue hysteresis loops at the cycle number of N = 1 and 600 correspond to the fiber/matrix interface slip Case 2, i.e. the fiber/matrix interface partially debonding and the fiber partially sliding relative to the matrix in the fiber/matrix interface debonded region; the fatigue hysteresis loop at the cycle number of N = 10000 corresponds to the fiber/matrix interface slip Case 3, i.e. the fiber/matrix interface completely debonding and the fiber partially sliding relative to the matrix in the fiber/matrix interface debonded region; and the fatigue hysteresis loop at the cycle number of N = 1000000 corresponds to the fiber/matrix interface slip Case 4, i.e. the fiber/matrix interface completely debonding and the fiber completely sliding relative to the matrix in the fiber/matrix interface debonded region. The experimental and predicted fatigue hysteresis dissipated energy versus the fiber/matrix interface frictional coefficient curves are shown in Fig. 2(b). The experimental fatigue hysteresis dissipated

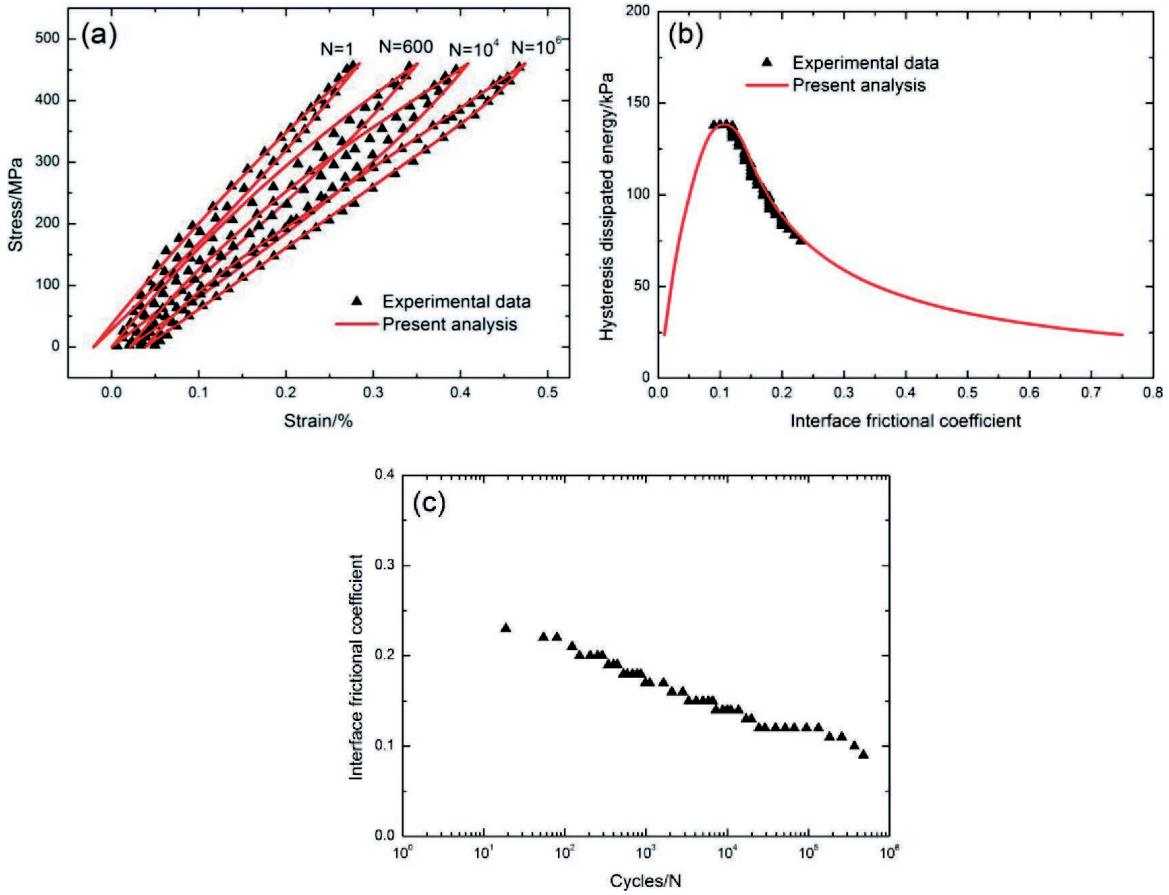

Fig. 2: (a) The experimental and theoretical fatigue hysteresis loops corresponding to different cycle numbers; (b) the experimental and theoretical fatigue hysteresis dissipated energy versus interface frictional coefficient curve; and (c) the interface frictional coefficient versus cycle number curve of type A unidirectional SiC/Si_3N_4 composite under $\sigma_{ma} = 460$ MPa at room temperature.

energy increases from 75 kJ/m^3 at the 18th applied cycle to the peak value of 138.2 kJ/m^3, and then decreases to 137.7 kJ/m^3 at the 479265th applied cycle, which lies in the right and left part of the theoretical fatigue hysteresis dissipated energy versus the fiber/matrix interface frictional coefficient curve. From comparison of the experimental fatigue hysteresis dissipated energy with theoretical computational values, the fiber/matrix interface frictional coefficient corresponding to different applied cycles can be obtained, as shown in Fig. 2(c). The fiber/matrix interface frictional coefficient decreases from 0.23 at the 18th applied cycle to 0.09 at the 479265th applied cycle.

For type B SiC/Si_3N_4 with weak fiber/matrix interface bonding at the fatigue peak stress of $\sigma_{max} = 460$ MPa, the experimental and predicted fatigue hysteresis loops corresponding to the cycle number of N = 2, 100, 300 and 500 are shown in Fig. 3(a), with the corresponding fiber/matrix interface frictional coefficient of $\mu = 0.16$, 0.1, 0.08 and 0.06. The fatigue hysteresis loops at the cycle number of N = 2 and 100 correspond to the fiber/matrix interface slip Case 2, i.e. the fiber/matrix interface partially debonding and the fiber partially sliding relative to the matrix in the fiber/matrix interface debonded region; and the fatigue hysteresis loops at the cycle number of N = 300 and 500 correspond to the fiber/matrix interface slip Case 3, i.e. the fiber/matrix interface completely debonding and the fiber completely sliding relative to the matrix in the fiber/matrix interface debonded region. The experimental fatigue hysteresis dissipated energy increases with applied cycles, i.e. from 99.6 kJ/m^3 at the 2nd applied cycle to 270 kJ/m^3 at the 550th applied cycle, which lies in the right part of the theoretical fatigue hysteresis dissipated energy versus the fiber/matrix interface frictional coefficient curve, as shown in Fig. 3(b). The fiber/matrix interface frictional coefficient corresponding to different applied cycles curve is shown in Fig. 3(c). The fiber/matrix interface frictional coefficient decreases from 0.16 at the 2nd applied cycle to 0.04 at the 550th applied cycle.

(b) *Elevated temperature*

Kotil [19] investigated the cyclic tension-tension fatigue behavior of unidirectional SiC/Si_3N_4 composite at 1000 °C. The fatigue tests were performed under load control at a sinusoidal waveform with the loading frequency of 10 Hz and the fatigue load ratio (i.e. minimum to maximum stress) of 0.1, and the maximum number of applied cycles was defined to be 2000000 applied cycles.

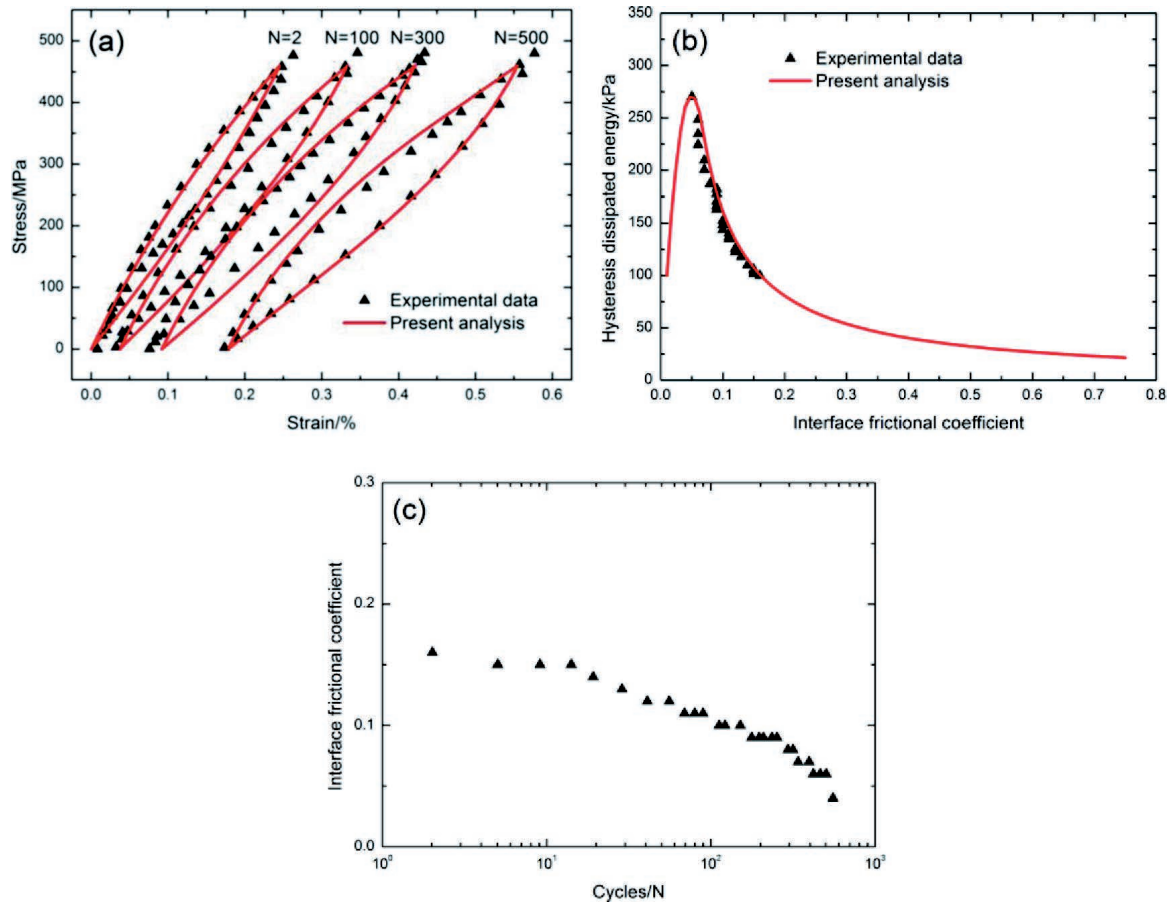

Fig. 3: (a) The experimental and theoretical fatigue hysteresis loops corresponding to different cycle numbers; (b) the experimental and theoretical fatigue hysteresis dissipated energy versus interface frictional coefficient curve; and (c) the interface frictional coefficient versus cycle number curve of type B unidirectional SiC/Si_3N_4 composite under $\sigma_{ma} = 460$ MPa at room temperature.

When the fatigue peak stress is $\sigma_{max} = 220$ MPa, the experimental and theoretical predicted fatigue hysteresis loops at the cycle number of N = 2500, 613000, 732000 and 740000 are shown in Fig. 4(a), with the corresponding fiber/matrix interface frictional coefficient of $\mu = 0.29$, 0.24, 0.17 and 0.11. The fatigue hysteresis loops at the cycle number of N = 2500, 613000 and 732000 correspond to the fiber/matrix interface slip Case 2, i.e. the fiber/matrix interface partially debonding and the fiber partially sliding relative to the matrix in the fiber/matrix interface debonded region; and the fatigue hysteresis loop at the cycle number of N = 740000 corresponds to the fiber/matrix interface slip Case 3, i.e. the fiber/matrix interface completely debonding and the fiber partially sliding relative to the matrix in the interface debonded region. The experimental and theoretical fatigue hysteresis dissipated energy versus the fiber/matrix interface frictional coefficient curves are shown in Fig. 4(b). The experimental fatigue hysteresis dissipated energy increases from 3.9 kJ/m^3 at the 2500th applied cycle to 10.1 kJ/m^3 at the 740000th applied cycle, which lies in the right part of the theoretical fatigue hysteresis dissipated energy versus the fiber/matrix interface frictional coefficient curve. The fiber/matrix interface frictional coefficient corresponding to different applied cycles curve is shown in Fig. 4(c). The fiber/matrix interface frictional coefficient decreases from 0.29 at the 2500th applied cycle to 0.11 at the 740000th applied cycle.

When the fatigue peak stress is $\sigma_{max} = 280$ MPa, the experimental and theoretical predicted fatigue hysteresis loops corresponding to the cycle number of N = 2000, 7000, 8000 and 33000 are illustrated in Fig. 5(a), with the corresponding fiber/matrix interface frictional coefficient of $\mu = 0.38$, 0.3, 0.15 and 0.02. The fatigue hysteresis loops at the cycle number of N = 2000 and 7000 correspond to the fiber/matrix interface slip Case 2, i.e. the fiber/matrix interface partially debonding and the fiber sliding partially relative to the matrix in the fiber/matrix interface debonded region; the fatigue hysteresis loop at the cycle number of N = 8000 corresponds to the fiber/matrix interface slip Case 3, i.e. the fiber/matrix interface completely debonding and the fiber sliding partially relative to the matrix in the interface debonded region; and the fatigue hysteresis loop at the cycle number of N = 33000 corresponds to the fiber/matrix interface slip Case 4, i.e., the fiber/matrix interface completely debonding and the fiber completely sliding relative to the matrix in the interface debonded region. The experimental and theoretical predicted fatigue hysteresis dissipated energy versus the fiber/matrix interface frictional coefficient curves are shown in Fig. 5(b). The experimental fatigue hysteresis dissipated

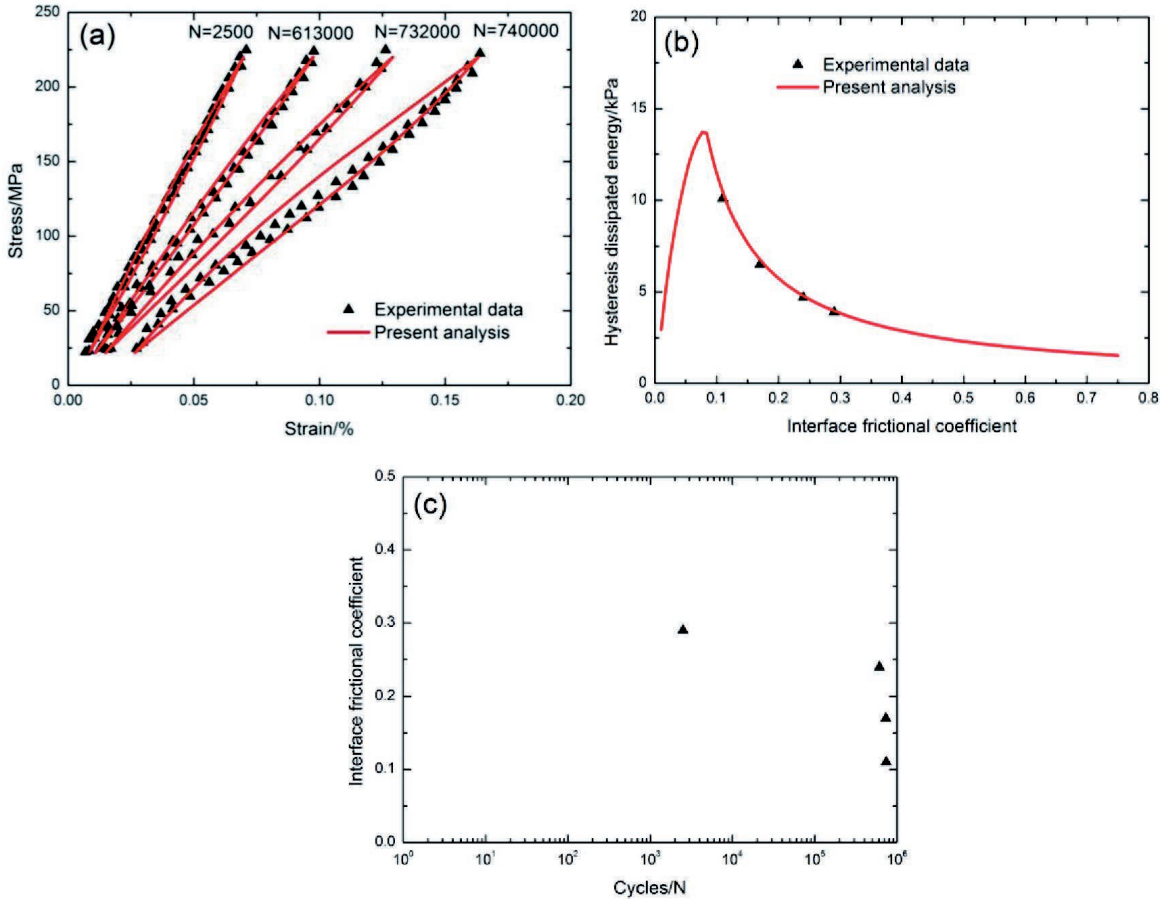

Fig. 4: (a) The experimental and theoretical fatigue hysteresis loops corresponding to different cycle numbers; (b) the experimental and theoretical fatigue hysteresis dissipated energy versus interface frictional coefficient curve; and (c) the interface frictional coefficient versus cycle number curve of unidirectional SiC/Si_3N_4 composite under $\sigma_{max} = 220$ MPa at 1000 °C.

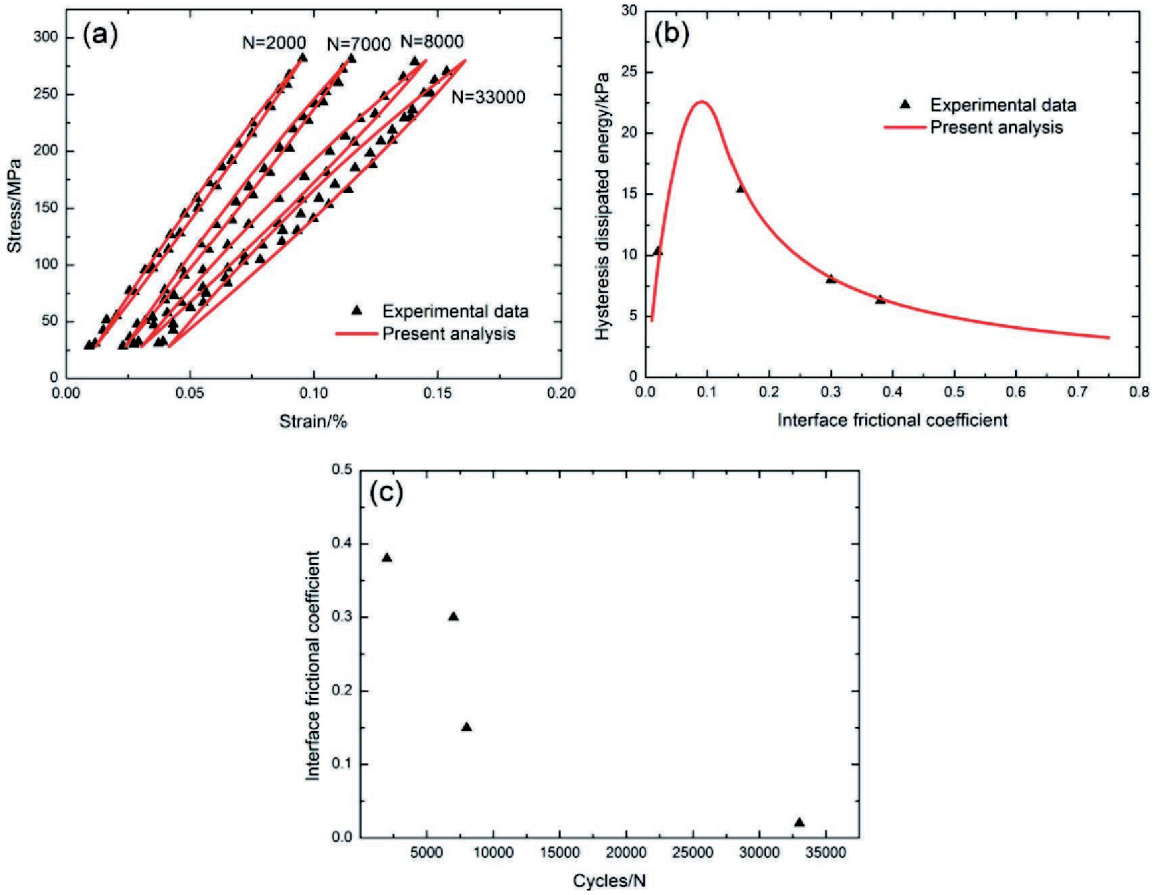

Fig. 5: (a) The experimental and theoretical fatigue hysteresis loops corresponding to different cycle numbers; (b) the experimental and theoretical fatigue hysteresis dissipated energy versus interface frictional coefficient curve; and (c) the interface frictional coefficient versus cycle number curve of unidirectional SiC/Si_3N_4 composite under σ_{max} = 280 MPa at 1000 °C.

energy increases from 6.3 kJ/m^3 at the 2000th applied cycle to 15.4 kJ/m^3 at the 8000th applied cycle, and then decreases to 10.3 kJ/m^3 at the 33000th applied cycle, which lies in the right and left part of the theoretical fatigue hysteresis dissipated energy versus the fiber/matrix interface frictional coefficient curve. The fiber/matrix interface frictional coefficient corresponding to different cycle number curve is shown in Fig. 5(c). The fiber/matrix interface frictional coefficient decreases from 0.38 at the 2000th applied cycle to 0.02 at the 33000th applied cycle.

(2) 2D woven SiC/SiC composite

(a) *Room temperature*

Reynaud [15] investigated the cyclic tension-tension fatigue behavior of 2D woven SiC/SiC composite at room temperature. The fatigue tests were performed under load control at a sinusoidal waveform with the loading frequency of 1 Hz and the fatigue load ratio (i.e. minimum to maximum stress) of 0, and the maximum number of applied cycles was defined to be 1000000 applied cycles.

When the fatigue peak stress is σ_{max} = 135 MPa, the experimental and theoretical predicted fatigue hysteresis loops at the cycle number of N = 100, 1000, 10000 and 100000 are shown in Fig. 6(a), with the corresponding fiber/matrix interface frictional coefficient of μ = 0.6, 0.42, 0.22 and 0.19. The fatigue hysteresis loops at the cycle number of N = 100, 1000, 10000 and 100000 correspond to the fiber/matrix interface slip Case 2, i.e. the fiber/matrix interface partially debonding and the fiber partially sliding relative to the matrix in the fiber/matrix interface debonded region. The experimental and theoretical fatigue hysteresis dissipated energy versus the fiber/matrix interface frictional coefficient curves are shown in Fig. 6(b). The experimental fatigue hysteresis dissipated energy increases from 6.5 kJ/m^3 at the 100th applied cycle to 20 kJ/m^3 at the 100000th applied cycle, which lies in the right part of the theoretical fatigue hysteresis dissipated energy versus the fiber/matrix interface frictional coefficient curve. The fiber/matrix interface frictional coefficient corresponding to different applied cycles curve is shown in Fig. 6(c). The fiber/matrix interface frictional coefficient decreases from 0.6 at the 100th applied cycle to 0.19 at the 100000th applied cycle.

(b) *Elevated temperature*

Reynaud [15] investigated the cyclic tension-tension fatigue behavior of 2D woven SiC/SiC composite at 600 °C, 800 °C, and 1000 °C in inert atmosphere. The fatigue peak stress was σ_{max} = 130 MPa, and the valley stress was σ_{min} = zero MPa. The loading frequency was f = 1 Hz.

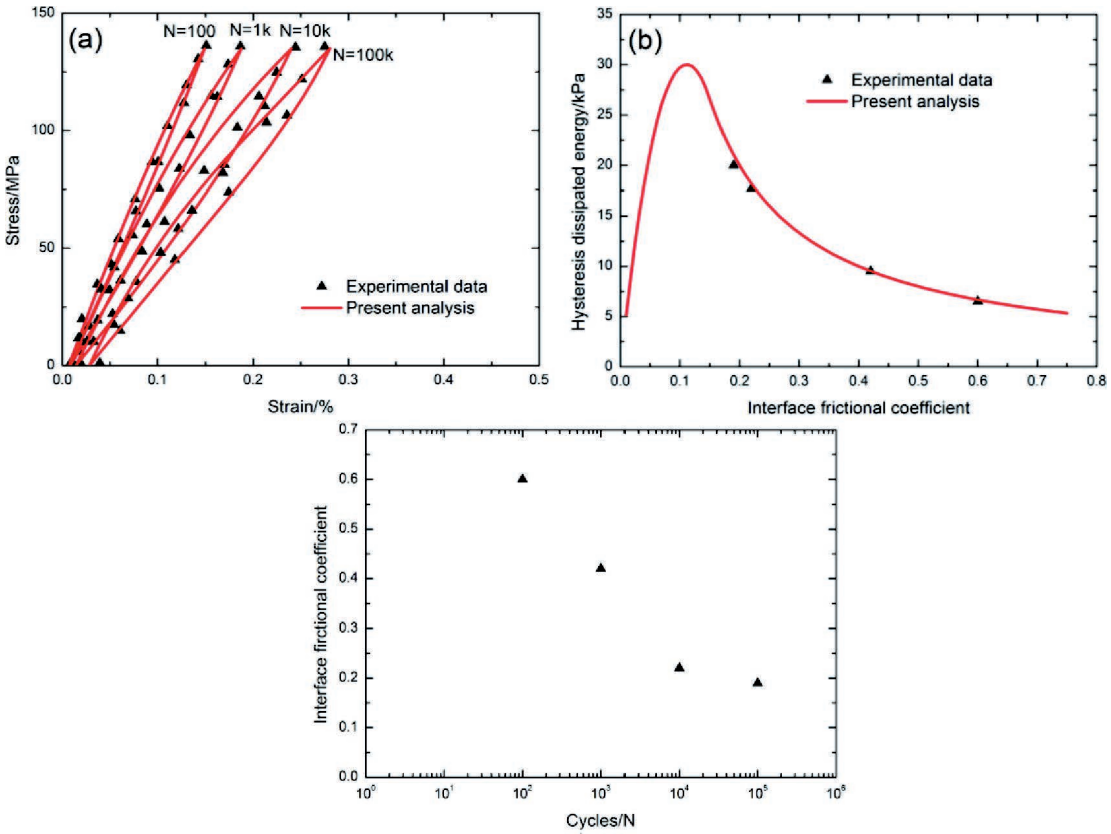

Fig. 6: (a) The experimental and theoretical fatigue hysteresis loops corresponding to different applied cycle numbers; (b) the experimental and theoretical fatigue hysteresis dissipated energy versus fiber/matrix interface frictional coefficient curve; and (c) the fiber/matrix interface frictional coefficient versus applied cycle number curve of 2D SiC/SiC composite under fatigue peak stress of $\sigma_{max} = 135$ MPa at room temperature.

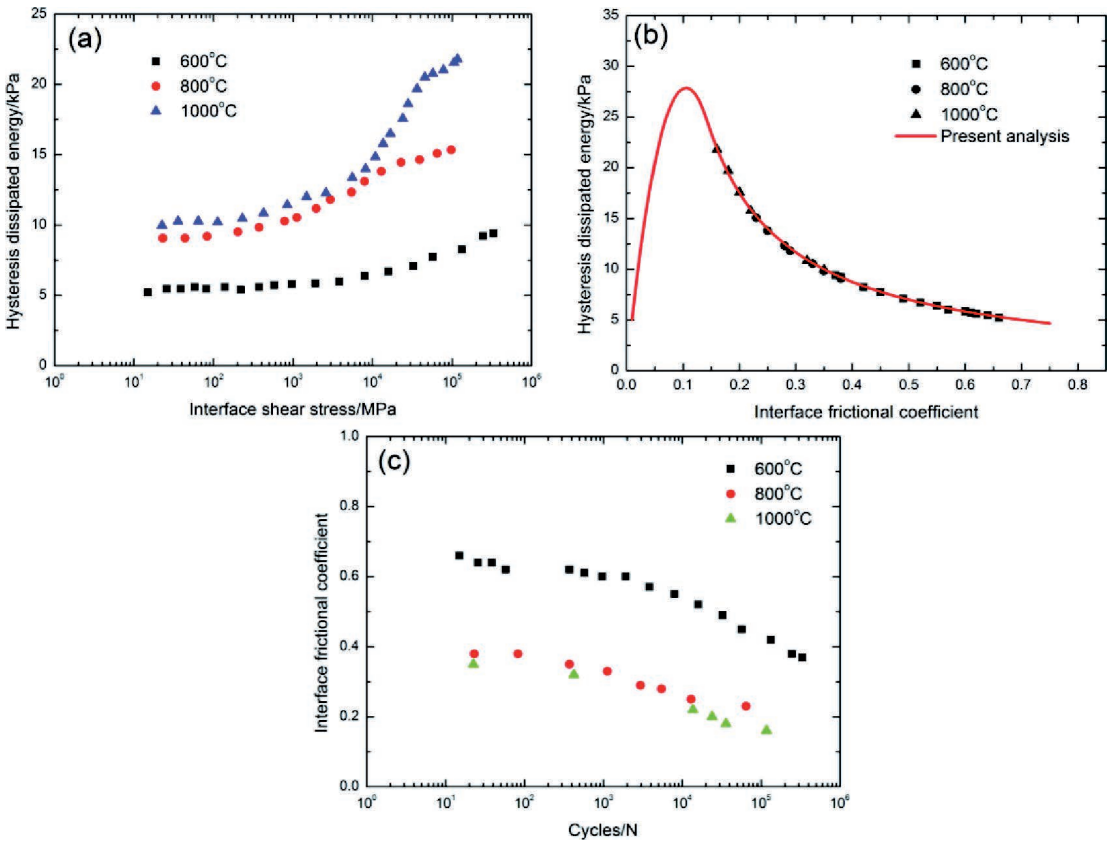

Fig. 7: (a) The experimental and theoretical fatigue hysteresis loops corresponding to different cycle numbers; (b) the experimental and theoretical fatigue hysteresis dissipated energy versus fiber/matrix interface frictional coefficient curve; and (c) the fiber/matrix interface frictional coefficient versus applied cycle number curve of 2D SiC/SiC composite under fatigue peak stress of $\sigma_{max} = 130$ MPa at 600 °C, 800 °C and 1000 °C in inert atmosphere.

Under fatigue peak stress of σ_{max} = 130 MPa, the experimental fatigue hysteresis dissipated energy versus cycle number curves at 600 °C, 800 °C and 1000 °C in inert atmosphere are shown in Fig. 7. The experimental fatigue hysteresis dissipated energy increases from 5.2 kPa at the 15th cycle to 9.4 kPa at the 333507th cycle at 600 °C, from 9 kPa at the 23th cycle to 15.3 kPa at the 97894th cycle at 800 °C, and from 10 kPa at the 22th cycle to 21.8 kPa at the 117055th cycle at 1000°C. The experimental and theoretical fatigue hysteresis dissipated energy versus the fiber/matrix interface frictional coefficient curve is shown in Fig. 7(b). The fatigue hysteresis dissipated energy increases from 4.6 kPa at μ = 0.75 to the peak value of 27.8 kPa at μ = 0.1, and then decreases to 5 kPa at μ = 0.01. The experimental fatigue hysteresis dissipated energy lies in the right part of the curve, corresponding to the fiber/matrix interface slip Case 2, i.e. the fiber/matrix interface partially debonding and the fiber partially sliding relative to the matrix in the fiber/matrix interface debonded region.

IV. Discussions

The experimental and theoretical fatigue hysteresis dissipated energy versus the fiber/matrix interface frictional coefficient curves of type A and type B SiC/Si_3N_4 composite under the same applied stress at room temperature, and SiC/Si_3N_4 composite under σ_{max} = 220 and 280 MPa at 1000 °C are illustrated in Fig. 8(a).

For SiC/Si_3N_4 with weak interface bonding at room temperature, the experimental fatigue hysteresis dissipated energy is higher and increases faster than that of the composite with strong interface bonding; the experimental fatigue hysteresis dissipated energy with strong interface bonding lies in the right and left part of the theoretical fatigue hysteresis dissipated energy versus the interface frictional coefficient curve; and the experimental fatigue hysteresis dissipated energy with weak interface bonding lies in the right part of the theoretical fatigue hysteresis dissipated energy curve.

For SiC/Si_3N_4 at the higher fatigue peak stress at 1000 °C, the experimental fatigue hysteresis dissipated energy is higher than that of the composite at the lower fatigue peak stress; the experimental fatigue hysteresis dissipated energy with high fatigue peak stress lies in the right and left part of the theoretical fatigue hysteresis dissipated energy curve; and the experimental fatigue hysteresis dissipated energy with low fatigue peak stress lies in the right of the theoretical fatigue hysteresis dissipated energy curve.

The fiber/matrix interface frictional coefficient versus cycle number curves of type A and type B SiC/Si_3N_4 composite under the same applied stress at room temperature, and SiC/Si_3N_4 composite under σ_{max} = 220 and 280 MPa at 1000 °C are illustrated in Fig. 8(b).

For SiC/Si_3N_4 with weak interface bonding, the interface frictional coefficient is lower than that of the composite with strong interface bonding, and the degradation rate of the interface frictional coefficient is also higher than that of the composite with strong interface bonding. For SiC/Si_3N_4 at the higher fatigue peak stress at 1000 °C, the interface frictional coefficient degradation rate is higher under the high fatigue peak stress than that under the low fatigue peak stress.

The experimental and theoretical fatigue hysteresis dissipated energy versus the fiber/matrix interface frictional coefficient curves of 2D SiC/SiC composite under σ_{max} = 135 MPa at room temperature and σ_{max} = 130 MPa at elevated temperature are shown in Fig. 9(a). With increasing fatigue peak stress, the fatigue hysteresis dissipated energy increases at the same fiber/matrix interface frictional coefficient when the fiber/matrix interface partially debonds; however, when the fiber/matrix interface completely debonds, the fatigue hysteresis dissipated energy under different peak stress approaches the same value.

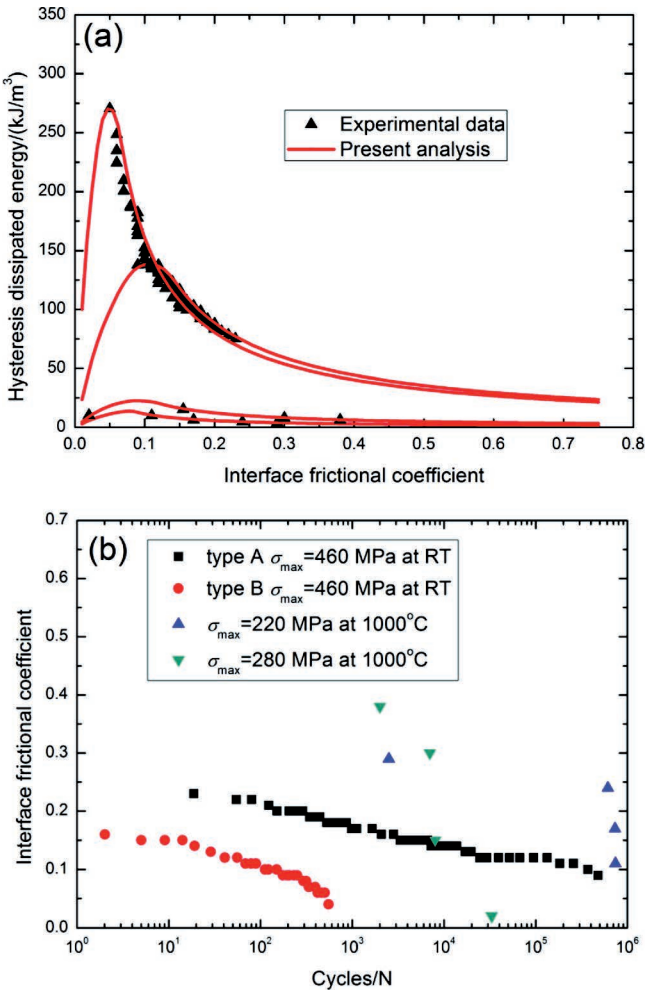

Fig. 8: (a) The experimental and theoretical fatigue hysteresis dissipated energy versus the fiber/matrix interface frictional coefficient curves; and (b) the fiber/matrix interface frictional coefficient versus cycle number curves of type A and type B SiC/Si_3N_4 composite under σ_{ma} = 460 at room temperature, and σ_{max} = 220 and 280 MPa at 1000 °C.

The experimental and theoretical fiber/matrix interface frictional coefficient versus applied cycle number curves of 2D SiC/SiC composite under σ_{max} = 135 MPa at room temperature and σ_{max} = 130 MPa at elevated temperature are shown in Fig. 9(b). The fiber/matrix interface frictional coefficient increases with decreasing testing temperature; and the degradation rate of the fiber/matrix interface frictional coefficient increases with increasing peak stress.

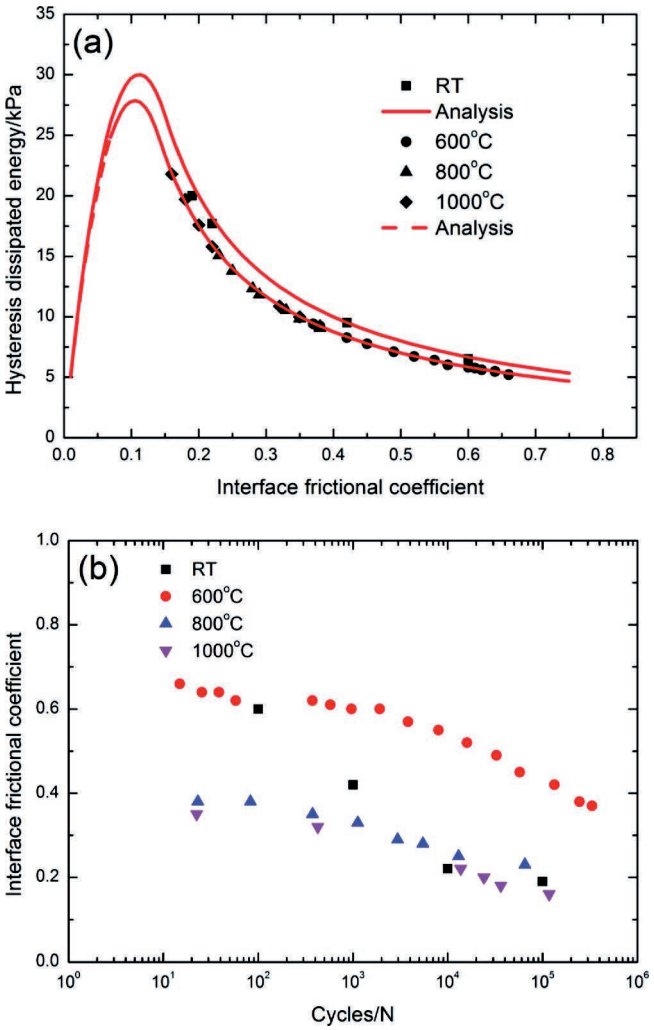

Fig. 9: (a) The experimental and theoretical fatigue hysteresis dissipated energy versus the fiber/matrix interface frictional coefficient curves; and (b) the fiber/matrix interface frictional coefficient versus cycle number curves of 2D SiC/SiC composite at room and elevated temperature.

V. Conclusions

In this paper, the fiber/matrix interfacial frictional coefficient in unidirectional SiC/Si_3N_4 and 2D woven SiC/SiC composites at room and elevated temperatures has been investigated. Fatigue hysteresis loops models considering the fiber/matrix interface friction were developed to establish the relationships between the fatigue hysteresis loops, fatigue hysteresis dissipated energy and the fiber/matrix interface frictional coefficient. With a comparison of the experimental fatigue hysteresis dissipated energy with theoretical computational values, the fiber/matrix interface frictional coefficient of SiC/Si_3N_4 and SiC/SiC composite at room and elevated temperatures has been obtained for different fiber/matrix interface bonding, cycle numbers and fatigue peak stresses. The evolution of fatigue hysteresis dissipated energy and the fiber/matrix interface frictional coefficient versus applied cycle numbers have been analyzed.

(1) For SiC/Si_3N_4 composite with weak interface bonding at room temperature, the experimental fatigue hysteresis dissipated energy is higher and increases faster than that of the composite with strong interface bonding; and the interface frictional coefficient is lower than that of the composite with strong interface bonding.

(2) For SiC/Si_3N_4 composite with high fatigue peak stress at 1000 °C, the fatigue hysteresis dissipated energy is higher than that of the composite with low fatigue peak stress, and lies in the right and left part of the theoretical fatigue hysteresis dissipated energy versus the interface frictional coefficient curve; and the degradation rate of the interface frictional coefficient is also higher than that of the composite with low fatigue peak stress.

(3) For SiC/SiC composite, with increasing fatigue peak stress, the fatigue hysteresis dissipated energy increases at the same fiber/matrix interface frictional coefficient when the fiber/matrix interface partially debonds; however, when the fiber/matrix interface completely debonds, the fatigue hysteresis dissipated energy under different peak stress approaches the same value.

Acknowledgements

The work reported here is supported by the Fundamental Research Funds for the Central Universities (Grant no. NS2016070).

References

1 Naslain, R.: Design, preparation and properties of non-oxide CMCs for application in engines and nuclear reactors: an overview, Compos. Sci. Technol., **64**, 155 – 170, (2004).

2 Li, L.B.: Modeling strength degradation of fiber-reinforced ceramic-matrix composites under cyclic loading at room and elevated temperatures, Mater. Sci. Eng. A, **695**, 221 – 229, (2017).

3 Holmes, J.W., Cho, C.D.: Experimental observations of frictional heating in fiber-reinforced ceramics, J. Am. Ceram. Soc., **75**, 929 – 938, (1992).

4 Rouby, D., Reynaud, P.: Fatigue behavior related to interface modification during load cycling in ceramic-matrix fiber composites, Comps. Sci. Technol., **48**, 109 – 118, (1993).

5 Evans, A.G., Zok, F.W., McMeeking, R.M.: Fatigue of ceramic matrix composites. Acta metall. mater., **43**, 859 – 875, (1995).

6 Brandstetter, J., Kromp, K., Peterlik, H., Weiss, R.: Effect of surface roughness on friction in fiber-bundle pull-out tests, Compos. Sci. Technol., **65**, 981 – 988, (2005).

7 Kuntz, M., Grathwahl, G.: Advanced evaluation of push-in data for the assessment of fiber reinforced ceramic matrix composites, Adv. Eng. Mater., **3**, 371 – 379, (2001).

8 Chandra, N., Ghonem, H.: Interfacial mechanics of push-out tests: theory and experiments, Compos. Part A, **32**, 575 – 584, (2001).

9 Li, L.B., Song, Y.D.: An approach to estimate interface shear stress of ceramic matrix composites from hysteresis loops, Appl. Compos. Mater., **17**, 309 – 328, (2010).

10 Solti, J.P., Robertson, D.D., Mall, S.: Estimation of interfacial properties from hysteresis energy loss in unidirectional ceramic matrix composites, Adv. Compos. Mater., **9**, 161 – 173, (2000).

11 Li, L.B., Reynaud, P., Fantozzi, G.: Tension-tension fatigue behavior of unidirectional SiC/Si_3N_4 composite with strong and weak interface bonding at room temperature. Ceram. Int., **43**, 8769 – 8777, (2017).

12 Sorensen, B.F., Talreja, R., Sorensen, O.T.: Micromechanical analysis of damage mechanisms in ceramic matrix composites during mechanical and thermal loading, Compos., **24**, 124 – 140, (1993).

13 Li, L.B., Song, Y.D.: Estimate interface frictional coefficient of ceramic matrix composites from hysteresis loops, J. Compos. Mater., **45**, 989 – 1006, (2010).

[14] Li, L.B.: Fatigue hysteresis behavior of unidirectional C/SiC ceramic-matrix composite at room and elevated temperatures., Mater. Sci. Eng. A, **625**, 1 – 18, (2015).

[15] Reynaud, P.: Cyclic fatigue of ceramic-matrix composites at ambient and elevated temperatures. Compos. Sci. Technol., **56**, 809 – 814, (1996).

[16] Dalmaz, A., Reynaud, P., Rouby, D., Fantozzi, G., Abbe, F.: Mechanical behavior and damage development during cyclic fatigue at high-temperature of a 2.5D carbon/SiC composite. Compos. Sci. Technol., **58**, 693 – 699, (1998).

[17] Fantozzi, G., Reynaud, P.: Mechanical hysteresis in ceramic matrix composites, Mater. Sci. Eng. A, **521 – 522**, 18 – 23, (2009).

[18] Olivier, C.: Fabrication and study of the mechanical behaviour of unidirectional composites C/Si_3N_4 et SiC/Si_3N_4, (in French), PhD Thesis, Lyon: INSA Lyon (1998).

[19] Kotil, T.: Ceramic composites: Experimental and analytical study of SiC/Si_3N_4 composites, PhD Thesis, Michigan: University of Michigan (1991).